The Astrophysical Journal, 944:173 (9pp), 2023 February 20 https://doi.org/10.3847/1538-4357/acb68a
© 2023. The Author(s). Published by the American Astronomical Society.
OPEN ACCESS

Synchrotron Pair Production Equilibrium in Relativistic Magnetic Reconnection

Alexander Y. Chen[1], Dmitri Uzdensky[2], and Jason Dexter[3]
[1] Physics Department and McDonnell Center for the Space Sciences, Washington University in St. Louis, MO 63130, USA; cuyran@wustl.edu
[2] Center for Integrated Plasma Studies, Department of Physics, University of Colorado Boulder, 390 UCB, Boulder, CO 80309-0390, USA
[3] JILA, University of Colorado and National Institute of Standards and Technology, 440 UCB, Boulder, CO 80309-0440, USA
Received 2022 September 7; revised 2023 January 25; accepted 2023 January 25; published 2023 February 22

Abstract

Magnetic reconnection is ubiquitous in astrophysical systems, and in many such systems the plasma suffers from significant cooling due to synchrotron radiation. We study relativistic magnetic reconnection in the presence of strong synchrotron cooling, where the ambient magnetization, σ, is high and the magnetic compactness, ℓ_B, of the system is of order unity. In this regime, $e^{\pm}$ pair production from synchrotron photons is inevitable, and this process can regulate the magnetization σ surrounding the current sheet. We investigate this self-regulation analytically and find a self-consistent steady state for a given magnetic compactness of the system and initial magnetization. This result helps estimate the self-consistent upstream magnetization in systems where plasma density is poorly constrained, and can be useful for a variety of astrophysical systems. As illustrative examples, we apply it to study the properties of reconnecting current sheets near the supermassive black hole of M87, as well as the equatorial current sheet outside the light cylinder of the Crab pulsar.

Unified Astronomy Thesaurus concepts: Plasma astrophysics (1261); Gamma-ray sources (633); Pulsars (1306); Black holes (162); Compact objects (288)

1. Introduction

Magnetic reconnection is a fundamental plasma physics process that dissipates magnetic energy into plasma heating and nonthermal particle acceleration. Over the past decade, significant progress in our understanding of collisionless relativistic reconnection has been made through first-principles particle-in-cell (PIC) simulations (e.g., Cerutti et al. 2012a; Guo et al. 2014; Sironi & Spitkovsky 2014; Werner et al. 2016, 2018). This process accelerates particles into a power-law energy distribution with index p and cutoff $\gamma_{\max}$ that depend on the upstream magnetization $\sigma = B_0^2/4\pi n_0 m_e c^2$ (e.g., Sironi & Spitkovsky 2014). In the ultra-relativistic limit of very high $\sigma \gg 1$, the power-law index p of the accelerated particles approaches unity, $p \to 1$ (Zenitani & Hoshino 2001; Lyubarsky & Liverts 2008; Guo et al. 2014; Werner et al. 2016).

However, the effects of radiation and their feedback to the process of magnetic reconnection have begun to be studied only recently (e.g., Jaroschek & Hoshino 2009; Uzdensky & McKinney 2011; Uzdensky et al. 2011; Cerutti et al. 2012a, 2014; Uzdensky & Spitkovsky 2014; Uzdensky 2016; Beloborodov 2017; Schoeffler et al. 2019; Hakobyan et al. 2019; Werner et al. 2019; Sironi & Beloborodov 2020; Mehlhaff et al. 2020; Sridhar et al. 2021; Mehlhaff et al. 2021). In extreme astrophysical environments, particles often suffer from significant radiative cooling through synchrotron or inverse Compton (IC) radiation. This can lead to significant changes to the power-law index of the particle energy spectra (Werner et al. 2016), and can produce observable intermittency through kinetic beaming (Cerutti et al. 2012b, 2013; Mehlhaff et al. 2020). In some systems, the radiated photons can be energetic enough to produce $e^{\pm}$ pairs in the upstream or close to the reconnecting current sheet, regulating the plasma supply and the magnetization parameter σ. Such systems include magnetospheres of rotation-powered pulsars (outside the light cylinder; e.g., Lyubarskii 1996; Hakobyan et al. 2019), magnetospheres and coronae of accreting black holes (e.g., Beloborodov 2017; Sironi & Beloborodov 2020; Sridhar et al. 2021; Mehlhaff et al. 2021), and active magnetospheres of magnetars (Uzdensky 2011; Beloborodov 2021).

For many of these astrophysical systems, the magnetization parameter σ can be poorly constrained, due to uncertainties in either the local magnetic field strength or plasma density. For example, the pair multiplicity injected by the Crab pulsar into its pulsar wind nebula is a long-standing problem (see, e.g., Amato 2014). The plasma density near the light cylinder can be quite uncertain and is likely regulated by local pair production (Hakobyan et al. 2019; Hu & Beloborodov 2022). For supermassive black holes, recent GRMHD simulations have shown that magnetically arrested disks (MADs) can undergo quasi-periodic eruptions that form transient current sheets in a low-density region near the black hole horizon (e.g., Chashkina et al. 2021; Ripperda et al. 2022; Scepi et al. 2022). However, due to artificial mass injection in MHD codes, it is difficult to constrain the magnetization in such an environment from first principles through simulations. This makes it difficult to make theoretical predictions about the radiative signatures of these current sheets.

In this paper, we investigate the effect of $e^{\pm}$ pair production from synchrotron photons in a reconnecting current sheet, and study how the plasma density self-regulates to an equilibrium. Section 2 defines the basic parameters of this problem and our assumptions. Section 3 presents an analytic model that captures the basic features of this self-regulation through pair production. Section 4 applies the model to two astrophysical scenarios: the supermassive black hole in M87 (Section 4.1) and the Crab pulsar (Section 4.2). Section 5 compares our results with previous works on related topics, and finally in

Original content from this work may be used under the terms of the Creative Commons Attribution 4.0 licence. Any further distribution of this work must maintain attribution to the author(s) and the title of the work, journal citation and DOI.

Section 6 we discuss some of the potential shortcomings of this model and possible future extensions.

2. Basic Parameters

One of the key dimensionless parameters that govern the magnetic reconnection physics is the upstream plasma magnetization:

$$\sigma \equiv \frac{B_0^2}{4\pi\rho_0 c^2}, \tag{1}$$

where B_0 is the reconnecting magnetic field strength, and $\rho_0 c^2$ is the rest-mass energy density of the upstream plasma. This definition assumes that the upstream is cold, or $kT \ll m_e c^2$, such that the relativistic enthalpy of the upstream plasma is primarily given by its rest mass.[4] This assumption is appropriate in an environment with strong cooling. We also limit our consideration to an $e^{\pm}$ plasma, which is appropriate in an environment where copious pair production is expected. Furthermore, we shall assume that reconnection proceeds in the relativistic regime, marked by $\sigma \gg 1$, expected in extreme astrophysical environments around black holes and neutron stars. Finally, in this paper we will focus on reconnection without a guide field, which is relevant to the applications that we will discuss in Section 4.

Relativistic reconnection-driven nonthermal particle acceleration in this so-called zero-guide-field case in a pair plasma has been well studied in many previous PIC studies, especially in the nonradiative case (e.g., Jaroschek et al. 2004; Zenitani & Hoshino 2007; Guo et al. 2014; Sironi & Spitkovsky 2014; Werner et al. 2016). In particular, it was found that particles undergo rapid primary acceleration in the elementary interplasmoid current layers around the X-points to a power-law energy distribution $f(\gamma) \sim \gamma^{-p}$, with a σ-dependent power-law index which approaches unity in the ultra-relativistic high-σ limit, $p(\sigma) \to 1$ as $\sigma \to \infty$ (see, e.g., Zenitani & Hoshino 2001; Larrabee et al. 2003; Lyubarsky & Liverts 2008; Werner et al. 2018). This primary power law extends up to around $\gamma_{\max} \sim 4\sigma$ (see, e.g., Werner et al. 2016; Uzdensky 2022), perhaps followed by a steeper higher-energy power-law spectrum (e.g., Petropoulou & Sironi 2018; Hakobyan et al. 2021), and finally by an exponential cutoff (Lyubarsky & Liverts 2008; Werner et al. 2016).

Synchrotron cooling introduces a second important dimensionless parameter, the magnetic compactness, ℓ_B, which measures the radiative energy loss rate of marginally relativistic ($\gamma \sim 1$) electrons with respect to the light-crossing time of the system:

$$\ell_B \equiv \frac{\sigma_T U_B L}{m_e c^2}, \tag{2}$$

where σ_T is the Thomson cross section, $U_B = B_0^2/8\pi$ is the magnetic energy density, and L is the system size, which we take to be the length of the current sheet.

For a given electron with Lorentz factor $\gamma \gg 1$ gyrating in a magnetic field with pitch angle $\theta = \pi/2$, its synchrotron cooling time is

$$t_{\rm cool} = \frac{\gamma m_e c^2}{4\sigma_T c \gamma^2 U_B/3}. \tag{3}$$

Equating this with the light-crossing time of the system, L/c, one can find that the electron will cool to a Lorentz factor of $\gamma_{\rm cool} \sim 1/\ell_B$ over the system light-crossing time if $\ell_B \lesssim 1$. If $\ell_B > 1$, the electron will become nonrelativistic before it leaves the system. The time for a particle with arbitrary initial Lorentz factor $\gamma \gg 1$ to cool down to $\gamma \sim 1$ is $t \sim L/c\ell_B$. In this paper, we study systems where $\ell_B \gtrsim 1$. In these systems synchrotron cooling is efficient, and leptons accelerated in the reconnection layer will cool to Lorentz factors $\gamma \sim 1$ before they exit the system. This also provides reasonable justification for our assumption that the upstream plasma is relativistically cold, $kT \ll m_e c^2$, in our definition of upstream magnetization σ (see Equation (1)).

When dealing with radiative reconnection, it is often beneficial to define a radiation-reaction-limited Lorentz factor by balancing the radiation reaction force with the accelerating electric force due to the typical reconnection electric field, $E_{\rm rec} = \beta_{\rm rec} B_0$:

$$\gamma_{\rm rad} \equiv \sqrt{\frac{3e\beta_{\rm rec} B_0}{4\sigma_T U_B}}, \tag{4}$$

where $\beta_{\rm rec} \simeq 0.1$ is the dimensionless collisionless relativistic reconnection rate. Since this quantity does not involve the system size L, it measures the *local* relative strength of radiative cooling. Note that since particles are accelerated near X-points deep inside the current layer, where the B field is small, their Lorentz factors can exceed $\gamma_{\rm rad}$ locally (Kirk 2004; Uzdensky et al. 2011; Cerutti et al. 2012a). Only once the particles encounter regions of strong perpendicular magnetic field, e.g., when they are captured in plasmoids, will they start radiating away most of their energy. The critical energy, $\gamma_{\rm rad}$, is related to ℓ_B by the system size:

$$\frac{4}{3}\gamma_{\rm rad}^2 \ell_B = \beta_{\rm rec}\frac{L}{\rho_0}, \tag{5}$$

where $\rho_0 = m_e c^2/eB_0$ is the nominal relativistic electron Larmor radius in the upstream field.

Finally, given a characteristic magnetic field, B_0, and electron Lorentz factor, γ, the characteristic synchrotron photon frequency is

$$\omega_c = \frac{3}{2}\gamma^2 \omega_B \sin\theta, \tag{6}$$

where $\omega_B = eB_0/m_e c$ is the standard nonrelativistic electron cyclotron frequency and θ is the particle's pitch angle. The synchrotron photon will be capable of creating an $e^{\pm}$ pair when its energy is larger than $m_e c^2$; or, in other words, when the Lorentz factor of the emitting particle is larger than

$$\gamma_c = \sqrt{\frac{2B_Q}{3B_0 \sin\theta}}, \tag{7}$$

where $B_Q \equiv m_e^2 c^3/e\hbar = 4.4 \times 10^{13}$ G is the quantum critical (Schwinger) magnetic field. If the plasma magnetization $\sigma \gtrsim \gamma_c/4$, so that $\gamma_{\max} \gtrsim \gamma_c$, then there will be an appreciable

[4] Otherwise, one will need to also define the "hot" magnetization, σ_h, using the full enthalpy of the upstream plasma, taking into account its relativistic internal energy and pressure.

number of reconnection-accelerated particles capable of radiating photons that can convert to pairs through photon–photon collisions.

3. Analytic Model

Consider a reconnecting current sheet with initial $\sigma_0 > \gamma_c \gg 1$ and thus capable of pair production through synchrotron photons. We are interested in the regime where synchrotron cooling is efficient, $\ell_B \gtrsim 1$. We expect that once reconnection begins, synchrotron photons start to create pairs in the vicinity of the current sheet, producing extra plasma that will regulate the effective upstream magnetization σ, reducing it from its initial, far-upstream value σ_0. The effective magnetization may then become smaller than γ_c, and this would strongly suppress pair production since particles would no longer be able to gain sufficient energy to emit pair-producing photons. This may lead to a limit cycle behavior, as was noted by Mehlhaff et al. (2021) in the case of IC radiation; this behavior is somewhat similar to a pair-producing gap in the magnetospheres of black holes and neutron stars (e.g., Chen & Yuan 2020; Kisaka et al. 2020). Alternatively, the system may be able to self-regulate to a quasi-steady state with an equilibrium $\sigma_\pm$. In this section, we quantitatively describe this process using a simple analytic model, and evaluate whether an asymptotic state will be reached.

Given an (assumed to be isotropic) photon distribution $n_\gamma(\epsilon) = n_\gamma f_\gamma(\epsilon)$, where $\epsilon = \hbar\omega_{\rm ph}/m_e c^2$ is the dimensionless photon energy and f_γ is normalized to unity, the pair-production rate can be calculated as

$$\dot{n}_\pm = \int n_\gamma f_\gamma(\epsilon)\nu_{\gamma\gamma}(\epsilon)d\epsilon, \tag{8}$$

where $\nu_{\gamma\gamma}$ is the γ–γ pair-production rate for a single photon of energy ϵ (Gould & Schreder 1967):

$$\nu_{\gamma\gamma}(\epsilon) = \iint \frac{1}{2} n_\gamma(\epsilon')\sigma_{\gamma\gamma} c(1 - \cos\theta)\sin\theta \, d\theta d\epsilon', \tag{9}$$

where $\sigma_{\gamma\gamma}$ is the total collision cross section for two photons of energies ϵ and ϵ' with relative angle θ. We assume magnetic reconnection produces a power-law photon spectrum:

$$f_\gamma = A\epsilon^{-(\alpha+1)} e^{-\epsilon/\epsilon_{\rm max}}, \tag{10}$$

which extends from $\epsilon_{\rm min}$ to $\epsilon_{\rm max}$ with an exponential cutoff above $\epsilon_{\rm max}$. The pair-production rate can then be written as (Svensson 1987)[5]

$$\nu_{\gamma\gamma}(\epsilon) \simeq c\sigma_T \eta(\alpha)\frac{n(1/\epsilon)}{\epsilon}, \tag{11}$$

where $\eta(\alpha)$ has an approximate form:

$$\eta(\alpha) \approx \frac{7}{6}(2 + \alpha)^{-1}(1 + \alpha)^{-5/3}. \tag{12}$$

The pair-production rate is dominated by the interaction of photons of energies ϵ and $1/\epsilon$. By integrating over the whole photon distribution, Equation (8) double-counts all potential pair-producing energy combinations; therefore, it is useful to set the lower limit of the integration to 1:

$$\begin{aligned}\dot{n}_\pm &\simeq n_\gamma^2 c\sigma_T \eta(\alpha) A^2 \int_1^\infty \frac{1}{\epsilon} e^{-\epsilon/\epsilon_{\rm max}} d\epsilon \\ &= n_\gamma^2 c\sigma_T \eta(\alpha) A^2 E_1(1/\epsilon_{\rm max}),\end{aligned} \tag{13}$$

where E_1 is the exponential integral, defined as $E_1(z) = \int_z^\infty t^{-1}e^{-t}\,dt$. It scales as $\log(\epsilon_{\rm max})$ when $\epsilon_{\rm max} \gg 1$, and drops to zero exponentially when $\epsilon_{\rm max} \ll 1$. Physically this means that $\dot{n}_\pm$ is exponentially suppressed when only the photons with energies significantly above the exponential cutoff are capable of producing pairs. Introducing an exponential cutoff allows us to gracefully handle the transition from $\epsilon_{\rm max} > 1$ to $\epsilon_{\rm max} < 1$. If we were to adopt a power-law distribution with a sharp cutoff at $\epsilon_{\rm max}$, then $\dot{n}_\pm$ would go to zero as soon as $\epsilon_{\rm max}$ drops below unity, which may have led to unrealistic conclusions. We have also assumed that $1/\epsilon_{\rm min} \gg \epsilon_{\rm max} \gg \epsilon_{\rm min}$, such that the upper limit in the integral in Equation (13) can be effectively taken to be infinity instead of $1/\epsilon_{\rm min}$. This assumption holds for the astrophysical applications that we explore in this paper.

We can estimate n_γ in general terms as follows. Consider reconnection as a process that converts a portion of magnetic energy into particle energy and eventually into radiation. The energy flux of photons away from the reconnection layer should equal to a certain fraction of the dissipated magnetic energy:

$$\begin{aligned}\langle\epsilon_{\rm ph}\rangle m_e c^2 n_\gamma c \sin\theta_b &= \kappa S = 2\kappa\beta_{\rm rec} c\frac{B_0^2}{4\pi} \\ &= 4\kappa\beta_{\rm rec} c U_B,\end{aligned} \tag{14}$$

where S is the Poynting flux into the current sheet, $\langle\epsilon_{\rm ph}\rangle$ is the mean photon energy normalized to $m_e c^2$, and κ is an efficiency factor that quantifies how much magnetic energy is converted to synchrotron radiation. In a radiatively efficient system, most of the dissipated magnetic energy is radiated away, hence κ essentially measures the amount of energy that is given to the plasma. PIC simulations have suggested that $\kappa \sim 0.5$ (see, e.g., Sironi & Beloborodov 2020), and we will adopt this fiducial value for our estimates. Next, the factor $\sin\theta_b$ accounts for the fact that synchrotron emission may have a degree of beaming with respect to the current sheet. We adopt $\sin\theta_b \simeq 0.5$ in our model, but acknowledge that it may be lower in reality. The leading factor of 2 accounts for incoming Poynting flux from both above and below the current sheet. Finally, $\beta_{\rm rec}$ is the normalized reconnection speed, which has been measured to be close to $\beta_{\rm rec} \sim 0.1$ in PIC simulations of relativistic reconnection.

Given the photon distribution described by Equation (10), we can directly compute $\langle\epsilon_{\rm ph}\rangle$:

$$\begin{aligned}\langle\epsilon_{\rm ph}\rangle &= A\int_{\epsilon_{\rm min}}^\infty \epsilon^{-\alpha} e^{-\epsilon/\epsilon_{\rm max}} d\epsilon \\ &\simeq A\left[\epsilon_{\rm max}^{-\alpha+1}\Gamma(1-\alpha) - \frac{\epsilon_{\rm min}^{-\alpha+1}}{1-\alpha} + O\left(\frac{\epsilon_{\rm min}}{\epsilon_{\rm max}}\right)^2\right].\end{aligned} \tag{15}$$

For $\alpha < 1$ and $\epsilon_{\rm max} \gg \epsilon_{\rm min}$, the expression simplifies to $\langle\epsilon_{\rm ph}\rangle \approx A\epsilon_{\rm max}^{1-\alpha}\,\Gamma(1-\alpha)$. In other words, the photon spectrum is dominated by the high-energy end. In the opposite regime

[5] This expression was derived without the exponential cutoff. However, in our application we mainly use the pair-production rate when $\epsilon > 1$, and $n(1/\epsilon)$ samples the low-energy part of the spectrum, insensitive to the exponential cutoff. Therefore we use this expression directly as an approximation.

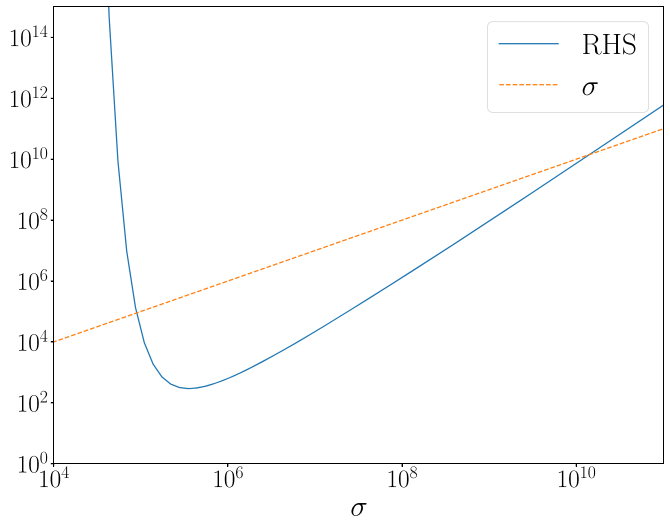

Figure 1. Example left- and right-hand sides of Equation (20), evaluated for $\ell_B = 1$, $\alpha = 0.5$, and $B = 100$ G. There are two solutions for σ where the two curves cross. The lower solution is stable while the upper solution is unstable.

where $\alpha > 1$, the spectrum is instead dominated by the low-energy end, and $\langle \epsilon_{\rm ph} \rangle \approx A \epsilon_{\rm min}^{\alpha-1}/(\alpha - 1)$. In realistic astrophysical systems where cooling is efficient, $\epsilon_{\rm min}$ can either approach the photon energy corresponding to the electron cyclotron frequency or be regulated by synchrotron self-absorption. On the other hand, $\epsilon_{\rm max}$ is determined by the nonthermal particle acceleration mechanism. The normalization constant A will eventually cancel out with the same factor in Equation (13).

Recent progress in PIC simulations of relativistic reconnection can inform us about the dependence of $\epsilon_{\rm max}$ and α on the upstream magnetization σ, since this synchrotron photon field is produced by the nonthermal particles accelerated in the current sheet. As discussed in Section 2, it has been shown that in the ultra-relativistic limit of very high $\sigma \gg 1$, the particles are promptly accelerated to a hard power-law distribution of index $p \sim 1$. This is the limit that is appropriate for the magnetospheres of compact objects, which we are ultimately interested in (see Section 4). However, since all leptons in the system will be fast-cooling if $\ell_B \gtrsim 1$, the cooled particle spectrum becomes $p \sim 2$ and the radiation spectrum then has a power-law index $\alpha = (p-1)/2 \sim 0.5$. In reality, the instantaneous particle spectrum in radiative reconnection is likely highly variable (see, e.g., Werner et al. 2019; Hakobyan et al. 2019), but the overall radiation spectrum is dominated by the times when the particle spectrum is hardest. Thus, $\alpha \sim 0.5$ can be a good approximation to the time-averaged photon spectrum, and we shall adopt this value in our analysis. In this limit, the mean photon energy becomes

$$\langle \epsilon_{\rm ph} \rangle \simeq 1.77 A \epsilon_{\rm max}^{0.5}. \tag{16}$$

The maximum extent of the power-law photon distribution, $\epsilon_{\rm max}$, is directly determined by the maximum extent, $\gamma_{\rm max}$, of the particle energy power law:

$$\epsilon_{\rm max} = \gamma_{\rm max}^2 \, b \sin\theta, \tag{17}$$

where $b \equiv B_0/B_Q$ is the dimensionless ratio of the upstream magnetic field to the Schwinger magnetic field, and θ is the average pitch angle of the particle distribution. For simplicity, we take a typical value of $\sin\theta = 1/2$. How the power-law cutoff $\gamma_{\rm max}$ depends on the reconnection physics is still an actively debated issue. The first serious study of this maximum extent of the power-law distribution was conducted by Werner et al. (2016), who found that $\gamma_{\rm max} \sim 4\sigma$, above which the particle distribution transitions to an exponential cutoff. More recently, Petropoulou & Sironi (2018) and Hakobyan et al. (2021) found that over time the system may develop a secondary power law above 4σ due to plasmoid compression; however, this effect was only demonstrated in 2D and it is not clear whether it persists in strongly radiative environments. In this paper we will adopt $\gamma_{\rm max} = 4\sigma$ and come back to this issue in Section 6. Under this assumption, the maximum extent of the power-law photon distribution can be written as $\epsilon_{\rm max} \simeq 8\sigma^2 b$.

We can now introduce $\langle \epsilon_{\rm ph} \rangle$ and $\epsilon_{\rm max}$ back into Equation (8) to recover an equation that only depends on the physical parameters of the reconnection layer and the upstream magnetization σ:

$$\begin{aligned} \dot{n}_\pm &= 16\kappa^2 \beta_{\rm rec}^2 \frac{U_B}{m_e c^2} \ell_B \frac{c}{L} \frac{\eta(\alpha) A^2 E_1(1/\epsilon_{\rm max})}{\langle \epsilon_{\rm ph} \rangle^2 \sin^2\theta_b}, \\ &\simeq 1.6 \times 10^{-3} \frac{U_B}{m_e c^2} \ell_B \frac{c}{L} \frac{E_1[(8\sigma^2 b)^{-1}]}{\sigma^2 b}, \end{aligned} \tag{18}$$

where we have made the substitutions $\kappa \approx 0.5$, $\beta_{\rm rec} \approx 0.1$, $\alpha \approx 0.5$, and $\sin\theta_b \approx 0.5$.

The balance between pair production and escape will determine the equilibrium plasma density and upstream magnetization. The pairs produced through collisions of synchrotron photons will in general escape in two ways: they will either stream along the upstream magnetic field at the speed of light and exit the system, or they will drift into the reconnecting current sheet at $v_{\rm rec} \simeq 0.1c$ and participate in the reconnection process. If pairs are predominately produced at a distance, d, from the current sheet that is larger than $\beta_{\rm rec} L$, then they will tend to escape the system before drifting into the reconnection layer, whereas if $d < \beta_{\rm rec} L$ the pairs will escape through drifting into the current sheet. In an environment with magnetic compactness $\ell_B \sim 1$, the characteristic optical depth to pair production can be estimated as

$$\tau_{\rm ph} = \frac{L}{l_{\rm ph}} \sim n_\gamma \sigma_T L \sim \beta_{\rm rec} \ell_B < 1. \tag{19}$$

As a result, $e^\pm$ pairs are typically produced far away from the current sheet and escape the system at the speed of light. This is the assumption that we will adopt in this analytic model. Under this assumption, the equilibrium number density of $e^\pm$ pairs is simply $n_\pm \simeq \dot{n}_\pm L/c$. This equilibrium density defines an effective magnetization via the equation[6]

$$\begin{aligned} \sigma_\pm \sim \frac{U_B}{n_\pm m_e c^2} &= \frac{\sin^2\theta_b}{16\kappa^2 \beta_{\rm rec}^2 \ell_B \eta(\alpha) A^2} \frac{\langle \epsilon_{\rm ph} \rangle^2}{E_1(1/\epsilon_{\rm max})} \\ &\simeq 6 \times 10^2 \frac{\sigma_\pm^2 b}{\ell_B E_1[(8\sigma_\pm^2 b)^{-1}]}. \end{aligned} \tag{20}$$

Equation (20) is a transcendental algebraic equation for the effective magnetization, $\sigma_\pm$, after synchrotron pair production

[6] Here we have also assumed that the density of created pairs is much higher than the ambient pair density (which thus becomes irrelevant), dominating the final plasma density. This assumption holds in the applications examined in Section 4.

has come to an equilibrium. In essence, we are looking for a pair-production equilibrium in a system where the number of pairs created directly correlates with the efficiency of nonthermal acceleration. Magnetic reconnection is an example of such a system, where the maximum particle acceleration correlates with σ, which in turn is determined by the numbers of $e^{\pm}$ pairs produced.

Figure 1 illustrates the general behavior of Equation (20). The right-hand side is a convex function and goes to infinity both when $\sigma \to 0$ and $\sigma \to \infty$. There are in general two solutions of the equation when the right-hand side crosses identity. The lower solution occurs close to the exponential suppression of the pair-production rate, where $\gamma_{\rm max} \sim \gamma_c$, while the upper solution occurs at a much larger σ, such that $\epsilon_{\rm max} \gg 1$. In the latter limit, $E_1(1/\epsilon_{\rm max}) \to \log(\epsilon_{\rm max})$, and the solution of Equation (20) approaches $\sigma_{\pm} \sim \ell_B/600b$.

However, the upper solution may not always be physical. Taking the result in Figure 1, for example, the upper solution is close to $\sigma \sim 1.4 \times 10^{10}$, at which point $\epsilon_{\rm max} \sim 3.6 \times 10^9$, far higher than the synchrotron burn-off limit of 160 MeV. In general, this solution is self-consistent only when the resulting σ is not too far above $\gamma_{\rm rad}$, so that the high-energy extent of the particle power law is controlled by σ and not by radiative cooling. Even when this upper solution is within the physical applicability of the model, it is still unstable: increasing σ from there decreases the pair-production rate (Equation (8)), triggering further increase of σ until reaching the background σ_0. This is because above this magnetization the hard radiation spectrum implies that there are not enough low-energy targets for the high-energy synchrotron photons to pair-create on. Decreasing σ from the upper solution, on the other hand, increases the pair-production rate and further decreases σ from the freshly generated $e^{\pm}$ plasma.

On the other hand, the lower solution is stable, and it is the solution that we seek. As mentioned above, this solution typically arises when $\gamma_{\rm max}$ is close to the pair-production threshold Lorentz factor γ_c (see Equation (7)), and further decreasing σ causes an exponential suppression in the pair-production rate. As long as the system starts off with a magnetization σ_0 between the two solutions, it will be driven toward the stable lower solution by self-regulated synchrotron pair production. Even though the initial σ_0 may be higher than the radiation-limited Lorentz factor $\gamma_{\rm rad}$, we find that this final equilibrium $\sigma_{\pm}$ is much smaller than $\gamma_{\rm rad}$ for a wide range of magnetic field strengths.

Figure 2 shows how the self-regulated magnetization $\sigma_{\pm}$ (lower solution) depends on upstream magnetic field B and the system compactness. The solution is obtained numerically using Newton's method. For a given magnetic compactness, Equation (20) ceases to have a solution when B is large enough, as its right-hand side no longer intersects with the identity line on Figure 1. In general, the two solutions approach each other at higher B fields. One can also see from Figure 2 that the equilibrium $\sigma_{\pm}$ depends much more sensitively on the magnetic field strength B than on the system size which manifests as ℓ_B. Qualitatively, this is because the lower solution is always pushed close to the pair-production threshold γ_c due to exponential suppression of the pair-production rate below it, and γ_c scales as $b^{-1/2}$ (see Equation (7)). In contrast, the equilibrium magnetization depends weakly on other parameters such as α and ℓ_B.

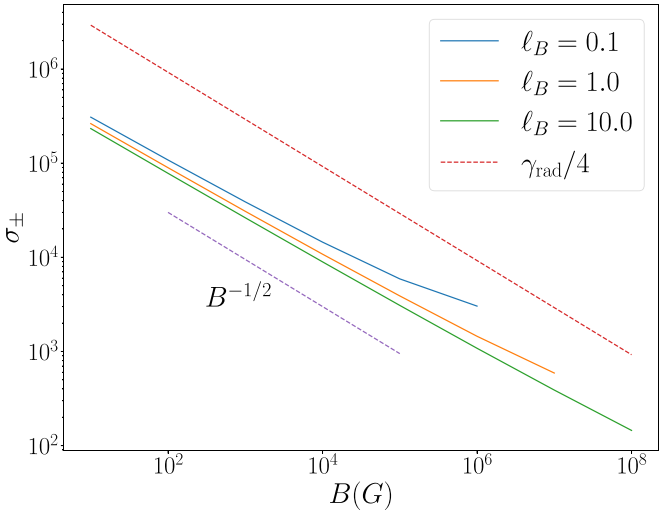

Figure 2. Dependence of the lower solution $\sigma_{\pm}$ on the upstream magnetic field B at different magnetic compactness ℓ_B, at $\alpha = 0.5$. For a wide range of magnetic field strengths, this solution is below the radiation-limited Lorentz factor $\gamma_{\rm rad}$. Note that with increasing B field, the two solutions become closer and beyond a certain point there is no longer a solution to Equation (20), which is close to where the curves terminate. For smaller compactness ℓ_B, this transition occurs at a lower magnetic field strength.

Note, however, that these results rely on the assumption that $\alpha < 1$, so that the photon spectrum peaks at the high-energy end. At high $\ell_B \gg 1$ or very strong cooling, this assumption may break; unfortunately, both the reconnection-accelerated particle spectrum and the radiation spectrum in this regime have not yet been sufficiently well studied in first-principles radiative PIC simulations and are thus still poorly understood. On the other hand, when $\ell_B \ll 1$, there is a spectral break for the synchrotron spectrum at low energies since particles with Lorentz factors $\gamma < 1/\ell_B$ do not cool appreciably before leaving the system. The spectral break changes the target photon distribution, and our simple assumption of Equation (11) needs to be replaced. Our analytic model proposed in this section works best when ℓ_B is not too far from unity.

4. Astrophysical Applications

We will now apply the analytic model described in Section 3 to two specific astrophysical scenarios where this process may prove to be relevant: a reconnecting current sheet in the magnetosphere of the central supermassive black hole of M87, and the equatorial current sheet outside the light cylinder of the Crab pulsar.

4.1. The Magnetosphere of M87

Recent GRMHD models and their comparison with the observations of the Event Horizon Telescope have significantly improved our understanding of the structures of accretion flow and the magnetic field close to the event horizon of the supermassive black hole at the center of M87 (Event Horizon Telescope Collaboration et al. 2019). MAD models seem to be favored by the recent polarization measurements (Event Horizon Telescope Collaboration et al. 2021). These MAD models tend to predict a magnetic field of $B \sim 1$–30 G in the millimeter-emission region. Depending on the numerical models, the magnetic field at the horizon can be as high as $B \sim 20$–200 G (Yao et al. 2021; Ripperda et al. 2022). At the same time, GRMHD simulations of the MAD model tend to

observe large-scale current sheets that can form in the equatorial plane near the event horizon during an eruption (see, e.g., Dexter et al. 2020; Chashkina et al. 2021; Porth et al. 2021; Scepi et al. 2022; Ripperda et al. 2022). High-resolution simulations show that these current sheets can be tearing-unstable and undergo magnetic reconnection, breaking up into a self-similar plasmoid chain (Ripperda et al. 2022). The length scales of these current sheets can be comparable to the black hole gravitational radius r_g. Taking $B \sim 200\,\mathrm{G}$ and $L \sim r_g \sim 10^{15}\,\mathrm{cm}$, we can estimate the system's magnetic compactness to be $\ell_B \sim 1.3$; therefore, synchrotron pair production can be an important factor that regulates local magnetization. The threshold Lorentz factor for synchrotron pair production under these conditions is $\gamma_c \sim 4 \times 10^5$ (Equation (7)), and the radiation-reaction-limited Lorentz factor is $\gamma_{\rm rad} \sim 2 \times 10^6$ (Equation (4)).

For these current sheet parameters, the two roots of Equation (20) are $\sigma_1 \approx 6 \times 10^4$ and $\sigma_2 \approx 2 \times 10^{10}$. The initial magnetization σ_0 in the magnetic bubble formed in an eruption of the MAD disk is very poorly constrained. Since the bubble material is torn from the low-density jet funnel, an upper limit for σ_0 can be estimated using the minimum Goldreich–Julian charge density, which screens local electric field (Goldreich & Julian 1969). For M87 near the horizon, $\sigma_{\rm GJ} \sim 10^{13}$ (Yao et al. 2021). However, it is unrealistic to expect that the plasma density is simply characterized by the Goldreich–Julian charge density, since Comptonized photons from the accretion disk can produce $e^{\pm}$ pairs in the jet funnel as well as in the vicinity of the horizon. This process is often called the "pair drizzle." Wong et al. (2021) recently calculated the pair-production rate from this drizzle mechanism and estimated that for M87 parameters $\dot{n}_{\pm} \sim 10^4 n_{\rm GJ}\, c/r_g$, which implies a much lower initial magnetization $\sigma_0 \sim 10^9$. Since this falls below our upper solution σ_2, our model predicts that pair production from synchrotron photons emitted by the particles accelerated in the reconnecting current layer will lower the magnetization to an equilibrium value of $\sigma_{\pm} \sim 6 \times 10^4$, which puts $\gamma_{\rm max} \sim 4\sigma_{\pm}$ close to γ_c and much lower than $\gamma_{\rm rad}$. This also implies a pair multiplicity of $\mathcal{M} = n_{\pm}/n_{\rm GJ} \sim 2 \times 10^8$ over the minimum Goldreich–Julian density. This result is similar in magnitude to what was estimated by Ripperda et al. (2022) and Kimura et al. (2022). However, our model predicts that the upstream magnetization will stabilize around this equilibrium value $\sigma_{\pm}$, which has implications for the M87 very-high-energy (VHE) gamma-ray flares.

It was proposed by Ripperda et al. (2022) that the MAD eruption events that form large-scale reconnecting current sheets may be a promising mechanism for powering the TeV flares observed from M87. However, our results disfavor this proposition, since synchrotron pair production will quickly lower the magnetization from its uncertain initial value to $\sim 6 \times 10^4$, which limits the extent of the power-law energy distribution to $\gamma_{\rm max} \sim 3 \times 10^5$. Electrons at this Lorentz factor are energetically incapable of producing TeV gamma rays, even if Compton scattering occurs in the deep Klein–Nishina regime. As a result, it is difficult for the system to produce a single power-law radiation spectrum that extends from several GeV up to several TeV. Since the equilibrium $\sigma_{\pm}$ scales approximately as $B^{-1/2}$ (Figure 2), a significantly lower magnetic field of $B \sim 2\,\mathrm{G}$ near the horizon is required to increase $\sigma_{\pm}$ to 6×10^5, which would then allow the particle energy power law to extend beyond a few TeV. However, such a low magnetic field would lead to a much lower dissipation power through the reconnection process: $L_{\rm rec} \sim U_B r_g^2 \beta_{\rm rec} c \sim 5 \times 10^{38}\,\mathrm{erg\,s^{-1}}$. This is much lower than the isotropic equivalent luminosity observed in M87 TeV flares, which can reach up to $\sim 10^{42}\,\mathrm{erg\,s^{-1}}$ (Abramowski et al. 2012).

Our synchrotron model does not take into account pairs produced by gamma-ray photons from IC scattering by the accelerated particles. These gamma-ray photons can be emitted through either the synchrotron self-Compton (SSC) mechanism or by electrons scattering the ambient lower-energy photons from the accretion disk. However, additional channels of pair production will only lower the final equilibrium magnetization, since there are more ways to generate plasma. This will, in general, make it even more difficult for the current sheet to produce TeV emission after pair production kicks in. We will discuss more about the potential role of SSC photons in Section 6.

4.2. Crab Pulsar

At the light cylinder of the Crab pulsar, the magnetic field is approximately $B_{\rm LC} \sim 4 \times 10^6\,\mathrm{G}$ (Uzdensky & Spitkovsky 2014). This is computed from the spin-down-inferred dipole moment and the rotation period of the pulsar. The size of the current sheet is given by the characteristic length scale, which is the light cylinder radius $R_{\rm LC} \sim 1.6 \times 10^8\,\mathrm{cm}$. The resulting system compactness is $\ell_B \sim 30$, close to the regime discussed in Section 3. The nominal magnetization σ_0 at the light cylinder is mostly determined by the copious $e^{\pm}$ outflow from the polar cap, and is generally believed to be 10^3–10^5 (Hakobyan et al. 2019). Fortunately, our analytic model is insensitive to this initial magnetization, as long as it lies within the two roots of Equation (20). For the parameters quoted above, the two roots are $\sigma_1 \approx 5 \times 10^2$ and $\sigma_2 \approx 9 \times 10^6$. This implies that if the current sheet starts with a magnetization within this range, synchrotron pair production will drive σ toward the lower root, which is $\sigma_{\pm} \approx 500$.

The Crab pulsar was observed to emit pulsed VHE gamma rays that form a power law extending up to TeV energies (Ansoldi et al. 2016). This puts the properties of its pulsed emission close to that of M87. Our predicted low $\sigma_{\pm} \sim 500$ would seemingly rule out the possibility that pairs accelerated in the equatorial current sheet can emit TeV gamma rays, even with a relativistic bulk-flow boost of $\Gamma \sim 100$. However, only a small fraction of the spin-down power of the Crab is needed to power the pulsed VHE emisssion, whereas in M87 the luminosity of VHE gamma-ray flares can be comparable to the jet power. It may be possible that these gamma rays are produced before the equilibrium $\sigma_{\pm}$ is reached.

Outside the light cylinder of the Crab pulsar, the current sheet feeds off the Y-point and always starts with plasma flowing from the inner magnetosphere with initial pair density $n_0 \gg n_{\rm GJ}$. This flow determines the initial magnetization σ_0 surrounding the current sheet that is much higher than our predicted $\sigma_{\pm}$. As pair production kicks in, the outflow magnetization will gradually drop and stabilize at around the self-regulated equilibrium $\sigma_{\pm}$ at some distance downstream of the Y-point. Since the gamma-ray spectrum from GeV to TeV appears to be a single power law (Ansoldi et al. 2016), we argue that almost all of these gamma rays are produced during this time, before the pair equilibrium is established. One can estimate a characteristic timescale for reaching this pair

equilibrium by computing the time it takes for the initial plasma density to double, normalized to the system light-crossing time:

$$\tau_{\pm} = \frac{n_0/\dot{n}_{\pm}}{L/c}. \quad (21)$$

One can evaluate this timescale using the pair-production rate (Equation (8)) and the initial magnetization σ_0. For Crab parameters, if we take an initial $\sigma_0 \sim 10^6$, which is required for particle acceleration up to TeV energies, this characteristic timescale is $\tau_{\pm} \sim 0.15$. One can take this dimensionless scale as the characteristic fraction of energy dissipated in the current sheet that can be emitted in high-energy (HE) to VHE gamma rays, since pair production will quickly lower σ such that the electron power law only extends to about a GeV. After pair production equilibrium is established, the synchrotron spectrum from these pairs only extends up to about MeV energies, which is a far cry from the observed pulsed gamma-ray component extending from 100 MeV to 1.5 TeV. If the current sheet dissipates about 10% of the spin-down power, $L_{\rm sd}$, between $R_{\rm LC}$ and $2R_{\rm LC}$ (Cerutti et al. 2020), then the expected gamma-ray luminosity $L_{\gamma} \lesssim 0.1\tau_{\pm}L_{\rm sd}$. Further accounting for the radiation spectrum and efficiency, this is close to the observed gamma-ray efficiency of the Crab pulsar of $L_{\gamma}/L_{\rm sd} \sim 10^{-3}$ (Abdo et al. 2013). A more detailed study on the pulsar gamma-ray spectrum, efficiency, and how it scales with the model parameters is beyond the scope of this paper, and will be deferred to a future work.

5. Comparison with Previous Work

Relatively few works have considered the effect of synchrotron pair production in the process of magnetic reconnection. Lyubarskii (1996) pointed out that the reconnecting current sheet outside the light cylinder can potentially power the high-energy emission from gamma-ray pulsars. He also calculated the number density of the $e^{\pm}$ plasma that would result from synchrotron pair production, and concluded that pair production will lower the magnetization σ surrounding the current sheet to the point where no gamma rays will be emitted. However, the detailed reconnection-driven particle acceleration mechanisms were not clearly understood at that time, and the present paper takes advantage of the recent development of our understanding of the magnetic reconnection process.

Hakobyan et al. (2019) performed PIC simulations with self-consistent synchrotron cooling and photon–photon pair production in the context of the Crab pulsar magnetosphere. However, their simulations were of a very limited parameter range and at low $\ell_B \sim 10^{-2}$. They derived a crude analytic model to predict the final number of pairs produced from the reconnecting current sheet, but did not consider the feedback of pair loading on the particle acceleration process itself. For Crab parameters, they found that the pair multiplicity η, defined as the ratio between the final number density and the initial upstream number density, can become as large as 10^5–10^6, which is greater than the initial magnetization σ_0 at the light cylinder, indicating that the final σ will become less than unity after pair production saturates. This implies that pair loading should strongly affect the particle acceleration process and in turn limit the final multiplicity. This is precisely the problem that we address in the present paper.

Beloborodov (2017, 2021) considered magnetic reconnection in the strongly radiative regime, with synchrotron pair production and IC emission in the context of the coronae of X-ray binaries, magnetar bursts, and electromagnetic precursors of binary neutron star mergers. His works focused more on the high magnetic compactness regime $\ell_B \gg 1$, which is relevant for these astrophysical systems. Our present work instead focuses on a different parameter regime of $\ell_B \sim 1$ and discusses the self-regulation of local magnetization through synchrotron pair production; consequently, it applies to a different set of astrophysical scenarios, as discussed in Section 4.

Schoeffler et al. (2019), similar to Hakobyan et al. (2019), used radiative QED-PIC simulations to study magnetic reconnection in the presence of strong synchrotron cooling and copious $e^{\pm}$ pair production in the context of pulsar and magnetar magnetospheres. However, the pair-production mechanism considered in their paper was photon interaction with a very strong (approaching B_Q) magnetic field, resulting in QED one-photon pair creation, which has a completely different pair-production cross section and rate. In that regime, synchrotron emission also approaches the quantum limit where $\epsilon_{\rm ph} \sim \gamma m_e c^2$, which alters the photon spectrum.

Mehlhaff et al. (2021) also studied radiative magnetic reconnection self-regulated by pair production using analytic methods, but their main interest was in $e^{\pm}$ pairs produced by IC photons emitted by reconnection-accelerated electrons upscattering an ambient photon field. They argued that, since the IC radiation and the subsequent pair production are from the same target mono-energetic photon field in the case under consideration, the IC scattering needs to be in the Klein–Nishina regime to be able to produce pairs, which affects the pair-production efficiency in these systems. Our study is similar in spirit but considers a different radiation mechanism, and thus applies to a different set of astrophysical systems.

Very recently, Kimura et al. (2022) performed a calculation of the synchrotron pair-production multiplicity during a magnetic reconnection event, which is similar to our present work, and applied it to low-luminosity active galactic nuclei including M87 and Sgr A*. They found that, for M87's parameters, once synchrotron pair production kicks in, it lowers the upstream magnetization to $\sigma \sim 8.7 \times 10^4$, similar to our estimates. However, they called this the "low-energy flaring state" and concluded that this state will not produce MeV photons efficiently, and that σ will grow again once the pairs are advected from the region. The reason for their conclusion was that they assumed reconnection only accelerates particles up to $\gamma \sim \sigma$, which will not allow synchrotron photons to pair-produce in this low-σ state. As we have shown in the present paper, even an exponential cutoff above $\gamma_{\rm max} \sim 4\sigma$ can allow the system to sustain a substantial level of pair production in this low-energy flaring state, making it difficult for the system to spontaneously go back to a state with high magnetization.

6. Discussion

We have considered synchrotron pair production in highly relativistic magnetic reconnection, and studied how the $e^{\pm}$ pairs feed back on the reconnection process itself, altering the magnetization close to the current sheet and ultimately reaching a self-regulated stable equilibrium $\sigma_{\pm}$. We found that this equilibrium is typically close to the threshold Lorentz factor for

synchrotron pair production, $4\sigma_{\pm} \sim \gamma_c$ (Equation (7)). In other words, the equilibrium magnetization is almost entirely determined by the local magnetic field strength. This process provides an estimate for the magnetization in finite-ℓ_B astrophysical systems where this quantity is poorly constrained, and we provided two examples of such systems: M87 and the Crab pulsar. In both cases, synchrotron pair production can reduce the initially very high magnetization to a much lower level, significantly constraining the power that can go into VHE gamma-ray emission.

Our model has adopted the assumption that relativistic magnetic reconnection impulsively accelerates particles to a hard power-law spectrum with index $p \sim 1$ and an exponential high-energy cutoff near $\gamma_{\rm max} \sim 4\sigma$. This coefficient of 4 was originally reported by Werner et al. (2016) and remains uncertain up to a factor of a few. The numerical value of this coefficient, however, turns out to be not too important in our model, since pair production tends to push $\gamma_{\rm max}$ close to γ_c. Changing the numerical coefficient to, for example, $\gamma_{\rm max} \sim 10\sigma$ only reduces the predicted final magnetization $\sigma_{\pm}$, but does not change the maximum extent of the particle/radiation power law. The results in Section 4 are mostly independent of the exact energy of the exponential cutoff.

Zhang et al. (2021) recently demonstrated that in 3D reconnection with moderate magnetization $\sigma = 10$, a secondary power law of $p \sim 1.5$ formed by free particles not captured by plasmoids can extend beyond $\gamma_{\rm max} \sim 4\sigma$, up to a cutoff energy that scales linearly with system size. When radiative cooling is significant, the secondary power law may extend up to around $\gamma_{\rm rad}$ instead. Approximately ~20% of the dissipated magnetic energy goes into this secondary power law. This effect may potentially change the conclusions of our model. Qualitatively, it will allow more pair-production activity at low σ, effectively pushing the equilibrium magnetization even lower. The secondary particle acceleration may also introduce a break in the radiation power law, which is not seen in the gamma-ray spectrum of M87. The quantitative effect of this secondary power law, especially at very high magnetization $\sigma_0 \gg 10$, will be studied in a future work.

In our model, we have neglected the change of the particle distribution, and hence of the synchrotron spectrum, caused by copious pair production. In particular, we have neglected the photons emitted by the secondary pairs. These photons in general will have lower energies, and may serve as target photons for the much higher-energy synchrotron photons close to the cutoff. However, near the final equilibrium $\sigma_{\pm}$ the power-law cutoff energy of synchrotron photons is already close to the pair-production threshold. Further increase of low-energy photon density will only enable photons in the exponential tail to create pairs, which will not meaningfully change the equilibrium magnetization. We have also neglected SSC photons that may pair-produce. However, since all synchrotron photons ultimately come from the dissipation of upstream magnetic energy, $U_{\rm ph} \lesssim \beta_{\rm rec} U_B$, one expects the SSC radiation energy density to be subdominant compared to the synchrotron energy density by a factor of $\beta_{\rm rec}$. Furthermore, SSC photons typically will have much higher energies than the synchrotron photons. Therefore, the density of their scatter targets should in general be lower in a hard power-law photon distribution with $\alpha < 1$. As a result, we expect SSC photons to play a subdominant role in regulating the pair-production equilibrium in a reconnection event. Recent work by Hakobyan et al. (2023) also finds that SSC radiation power is significantly lower than the synchrotron power, limiting their contribution to the $e^{\pm}$ pair density.

PIC simulations that incorporate photon–photon pair production, similar to what was done by Hakobyan et al. (2019) but in the regime of $\ell_B \sim 1$, will help verify the validity of the analytic model presented in the present work. Such time-dependent simulations will also capture the whole process of photon emission and pair production, and will be able to measure how the upstream magnetization responds to it. The results may place a more quantitative bound on the gamma-ray luminosity from the relativistic reconnecting current sheet before it is overwhelmed by $e^{\pm}$ pairs, therefore providing more detailed estimates of the HE to VHE gamma-ray luminosity and spectra from these systems.

We thank Yajie Yuan and Andrei Beloborodov for helpful discussions, and Sasha Philippov and John Mehlhaff for helpful comments on the manuscript. A.C. and J.D. acknowledge support from Fermi Guest Investigation grant No. 80NSSC21K2027. A.C. also acknowledges support from NSF grant No. DMS-2235457. This work was also supported by NSF grant Nos. AST-1806084 and AST-1903335, and by NASA grant Nos. 80NSSC20K0545 and 80NSSC22K0828. This work was stimulated by the discussions in the Fourth Purdue Workshop on Relativistic Plasma Astrophysics in 2022 May.

ORCID iDs

Alexander Y. Chen https://orcid.org/0000-0002-4738-1168
Jason Dexter https://orcid.org/0000-0003-3903-0373

References

Abdo, A. A., Ajello, M., Allafort, A., et al. 2013, ApJS, 208, 17
Abramowski, A., Acero, F., Aharonian, F., et al. 2012, ApJ, 746, 151
Amato, E. 2014, IJMPC, 28, 1460160
Ansoldi, S., Antonelli, L. A., Antoranz, P., et al. 2016, A&A, 585, A133
Beloborodov, A. M. 2017, ApJ, 850, 141
Beloborodov, A. M. 2021, ApJ, 921, 92
Cerutti, B., Philippov, A. A., & Dubus, G. 2020, A&A, 642, A204
Cerutti, B., Uzdensky, D. A., & Begelman, M. C. 2012a, ApJ, 746, 148
Cerutti, B., Werner, G. R., Uzdensky, D. A., & Begelman, M. C. 2012b, ApJL, 754, L33
Cerutti, B., Werner, G. R., Uzdensky, D. A., & Begelman, M. C. 2013, ApJ, 770, 147
Cerutti, B., Werner, G. R., Uzdensky, D. A., & Begelman, M. C. 2014, ApJ, 782, 104
Chashkina, A., Bromberg, O., & Levinson, A. 2021, MNRAS, 508, 1241
Chen, A. Y., & Yuan, Y. 2020, ApJ, 895, 121
Dexter, J., Tchekhovskoy, A., Jimenez-Rosales, A., et al. 2020, MNRAS, 497, 4999
Event Horizon Telescope Collaboration, Akiyama, K., Alberdi, A., et al. 2019, ApJL, 875, L1
Event Horizon Telescope Collaboration, Akiyama, K., Algaba, J. C., et al. 2021, ApJL, 910, L13
Goldreich, P., & Julian, W. H. 1969, ApJ, 157, 869
Gould, R. J., & Schreder, G. P. 1967, PhRv, 155, 1404
Guo, F., Li, H., Daughton, W., & Liu, Y.-H. 2014, PhRvL, 113, 155005
Hakobyan, H., Petropoulou, M., Spitkovsky, A., & Sironi, L. 2021, ApJ, 912, 48
Hakobyan, H., Philippov, A., & Spitkovsky, A. 2019, ApJ, 877, 53
Hakobyan, H., Ripperda, B., & Philippov, A. 2023, ApJL, 943, L29
Hu, R., & Beloborodov, A. M. 2022, ApJ, 939, 42
Jaroschek, C. H., & Hoshino, M. 2009, PhRvL, 103, 075002
Jaroschek, C. H., Treumann, R. A., Lesch, H., & Scholer, M. 2004, PhPl, 11, 1151

Kimura, S. S., Toma, K., Noda, H., & Hada, K. 2022, ApJL, 937, L34
Kirk, J. G. 2004, PhRvL, 92, 181101
Kisaka, S., Levinson, A., & Toma, K. 2020, ApJ, 902, 80
Larrabee, D. A., Lovelace, R. V. E., & Romanova, M. M. 2003, ApJ, 586, 72
Lyubarskii, Y. E. 1996, A&A, 311, 172
Lyubarsky, Y., & Liverts, M. 2008, ApJ, 682, 1436
Mehlhaff, J. M., Werner, G. R., Uzdensky, D. A., & Begelman, M. C. 2020, MNRAS, 498, 799
Mehlhaff, J. M., Werner, G. R., Uzdensky, D. A., & Begelman, M. C. 2021, MNRAS, 508, 4532
Petropoulou, M., & Sironi, L. 2018, MNRAS, 481, 5687
Porth, O., Mizuno, Y., Younsi, Z., & Fromm, C. M. 2021, MNRAS, 502, 2023
Ripperda, B., Liska, M., Chatterjee, K., et al. 2022, ApJL, 924, L32
Scepi, N., Dexter, J., & Begelman, M. C. 2022, MNRAS, 511, 3536
Schoeffler, K. M., Grismayer, T., Uzdensky, D., Fonseca, R. A., & Silva, L. O. 2019, ApJ, 870, 49
Sironi, L., & Beloborodov, A. M. 2020, ApJ, 899, 52
Sironi, L., & Spitkovsky, A. 2014, ApJL, 783, L21
Sridhar, N., Sironi, L., & Beloborodov, A. M. 2021, MNRAS, 507, 5625
Svensson, R. 1987, MNRAS, 227, 403
Uzdensky, D. A. 2011, SSRv, 160, 45
Uzdensky, D. A. 2016, in Magnetic Reconnection, Astrophysics and Space Science Library, ed. W. Gonzalez & E. Parker, 427 (Switzerland: Springer), 473
Uzdensky, D. A. 2022, JPlPh, 88, 905880114
Uzdensky, D. A., Cerutti, B., & Begelman, M. C. 2011, ApJL, 737, L40
Uzdensky, D. A., & McKinney, J. C. 2011, PhPl, 18, 042105
Uzdensky, D. A., & Spitkovsky, A. 2014, ApJ, 780, 3
Werner, G. R., Philippov, A. A., & Uzdensky, D. A. 2019, MNRAS, 482, L60
Werner, G. R., Uzdensky, D. A., Begelman, M. C., Cerutti, B., & Nalewajko, K. 2018, MNRAS, 473, 4840
Werner, G. R., Uzdensky, D. A., Cerutti, B., Nalewajko, K., & Begelman, M. C. 2016, ApJL, 816, L8
Wong, G. N., Ryan, B. R., & Gammie, C. F. 2021, ApJ, 907, 73
Yao, P. Z., Dexter, J., Chen, A. Y., Ryan, B. R., & Wong, G. N. 2021, MNRAS, 507, 4864
Zenitani, S., & Hoshino, M. 2001, ApJL, 562, L63
Zenitani, S., & Hoshino, M. 2007, ApJ, 670, 702
Zhang, H., Sironi, L., & Giannios, D. 2021, ApJ, 922, 261